HAL
open science

Oxidation of Si nanocrystals fabricated by ultralow-energy ion implantation in thin SiO2 layers

H. Coffin, Caroline Bonafos, Sylvie Schamm-Chardon, Nikolay Cherkashin, Gérard Benassayag, Alain Claverie, Marc Respaud, P. Dimitrakis, P. Normand

▶ To cite this version:

H. Coffin, Caroline Bonafos, Sylvie Schamm-Chardon, Nikolay Cherkashin, Gérard Benassayag, et al.. Oxidation of Si nanocrystals fabricated by ultralow-energy ion implantation in thin SiO2 layers . Journal of Applied Physics, 2006, 99 (4), pp.044302. 10.1063/1.2171785 . hal-01736074

HAL Id: hal-01736074

https://hal.science/hal-01736074v1

Submitted on 23 Mar 2018

HAL is a multi-disciplinary open access archive for the deposit and dissemination of scientific research documents, whether they are published or not. The documents may come from teaching and research institutions in France or abroad, or from public or private research centers.

L'archive ouverte pluridisciplinaire **HAL**, est destinée au dépôt et à la diffusion de documents scientifiques de niveau recherche, publiés ou non, émanant des établissements d'enseignement et de recherche français ou étrangers, des laboratoires publics ou privés.

Oxidation of Si nanocrystals fabricated by ultralow-energy ion implantation in thin SiO_2 layers

H. Coffin, C. Bonafos, S. Schamm, N. Cherkashin, G. Ben Assayag, A. Claverie, M. Respaud, P. Dimitrakis, and P. Normand

Citation: Journal of Applied Physics **99**, 044302 (2006); doi: 10.1063/1.2171785
View online: https://doi.org/10.1063/1.2171785
View Table of Contents: http://aip.scitation.org/toc/jap/99/4
Published by the American Institute of Physics

Articles you may be interested in

Modeling stress retarded self-limiting oxidation of suspended silicon nanowires for the development of silicon nanowire-based nanodevices
Journal of Applied Physics **110**, 033524 (2011); 10.1063/1.3611420

General Relationship for the Thermal Oxidation of Silicon
Journal of Applied Physics **36**, 3770 (1965); 10.1063/1.1713945

Plastic analysis of cylinder oxidation
Applied Physics Letters **54**, 1815 (1989); 10.1063/1.101248

Thermal oxidation of silicon nanocrystals in O_2 and NO ambient
Journal of Applied Physics **93**, 5637 (2003); 10.1063/1.1565172

Oxidation property of silicon small particles
Applied Physics Letters **58**, 1662 (1991); 10.1063/1.105129

Self-limiting oxidation for fabricating sub-5 nm silicon nanowires
Applied Physics Letters **64**, 1383 (1994); 10.1063/1.111914

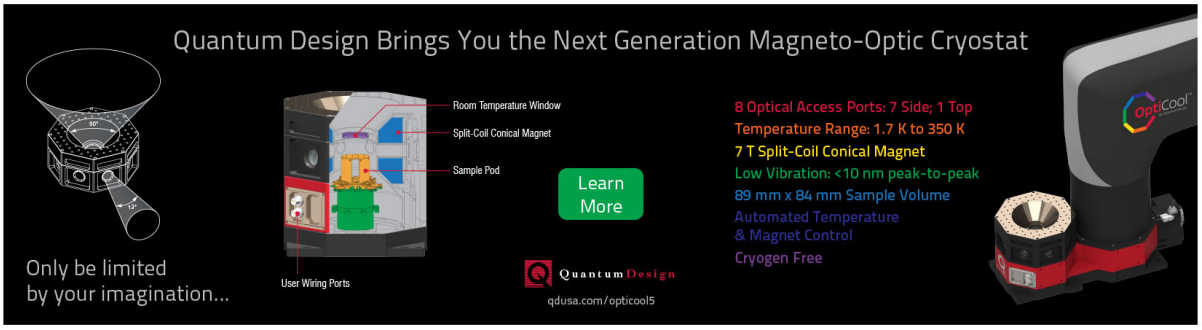

Oxidation of Si nanocrystals fabricated by ultralow-energy ion implantation in thin SiO_2 layers

H. Coffin, C. Bonafos,[a] S. Schamm, N. Cherkashin,[b] G. Ben Assayag, and A. Claverie
CEMES-CNRS, 29 rue J. Marvig, 31055 Toulouse, France

M. Respaud
LNMO, INSA, Département de Physique, 135 Avenue de Rangueil, 31077 Toulouse, France

P. Dimitrakis and P. Normand
Institute of Microelectronics, NCSR "Demokritos," 15310 Aghia Praskevi, Greece

(Received 29 July 2005; accepted 10 January 2006; published online 16 February 2006)

The effect of thermal treatments in nitrogen-diluted oxygen on the structural characteristics of two-dimensional arrays of Si nanocrystals (NCs) fabricated by ultralow-energy ion implantation (1 keV) in thin silicon dioxide layers is reported. The NC characteristics (size, density, and coverage) have been measured by spatially resolved electron-energy-loss spectroscopy by using the spectrum-imaging mode of a scanning transmission electron microscope. Their evolution has been studied as a function of thermal treatment duration at a temperature (900 °C) below the SiO_2 viscoelastic point. An extended spherical Deal-Grove [J. Appl. Phys. **36**, 3770 (1965)] model for self-limiting oxidation of embedded silicon NCs has been carried out. It proposes that the stress effects, due to oxide deformation, slow down the NC oxidation rate and lead to a self-limiting oxide growth. The model predictions show a good agreement with the experimental results. Soft oxidation appears to be a powerful way for manipulating the NC size distribution and surface density. © *2006 American Institute of Physics*. [DOI: 10.1063/1.2171785]

I. INTRODUCTION

A nanocrystal (NC) memory cell consists of a metal-oxide-semiconductor field-effect transistor (MOSFET) with monodisperse nanometer-scale crystals embedded within the gate dielectric.[1] By associating the finite-size effects of NCs and the benefits (robustness and fault tolerance) of a stored charge distribution, NC memories offer an attractive alternative for extending the scaling of conventional floating-gate memories (e.g., flash nonvolatile memories). Various NC materials and NC self-assembling techniques have been explored in the last few years. A substantial amount of investigation has gone into Si, Ge, or SiGe materials using different deposition techniques,[1,2] thermal oxidation of $Si_{1-x}Ge_x$,[3] or ion implantation followed by annealing.[4,5] The possibility of fabricating Si NCs in thin SiO_2 films by ultralow-energy Si implantation and subsequent thermal treatment has been recently demonstrated.[6,7] This fabrication route is very attractive because of its ability to control the size and location of a narrow NC band and its compatibility with standard complementary metal-oxide semiconductor (CMOS) processes. In practice, high-dose (typically 10^{16} cm^{-2}) Si implantation in the 1 keV range into very thin (<10 nm) oxide layers followed by annealing at temperatures in the 900–1000 °C range allows for the formation of two-dimensional (2D) arrays of Si NCs at tunable tunneling distances from the SiO_2/Si interface.[6] As shown in Ref. 7, it is possible to accurately control the position of the NC band by changing the implantation and annealing conditions. In addition, Si-NC gate stacks with improved electrical performance have been obtained recently by carrying out the annealing step under slight oxidizing conditions.[8] Such conditions restore significantly the integrity of the oxide and lead to gate stacks suitable for nonvolatile memory devices operating at low voltages.[9] Annealing in oxidizing conditions affects also the NC population.[10] As a consequence the oxidation step can be used for monitoring the size, density, and surface fraction of the NC population and thus for controlling the memory performance of the final devices. It is expected that below the viscoelastic temperature of SiO_2 (950 °C),[11,12] the oxidation of nonplanar Si structures is retarded due to normal stress induced at the Si/SiO_2 interface,[13–16] thus leading to self-limiting size effects. The aim of this work is to study and model the thermal oxidation of Si NCs embedded in SiO_2. NC oxidation is examined as a function of the duration of thermal treatments performed at 900 °C in nitrogen-diluted-oxygen ambient (N_2+1.5% O_2). The NC characteristics (size and aerial density) have been extracted from filtered images obtained by using the spectrum-imaging mode of a scanning transmission electron microscope (STEM). The swelling of the SiO_2 layer due to NC oxidation has been measured on cross-sectional transmission electron microscopy (TEM) images. In addition, we have extended the one-dimensional (1D) Deal and Grove model[17] to spherical geometry in order to properly model the Si NC evolution under oxidation. This model assumes that stress effects associated with nonuniform deformation of the oxide by viscous flow reduce the oxidation rate. Based on the work of Kao *et al.*[13,14] and Omachi *et al.*,[16] it predicts the retardation of oxide growth on a curved surface. This retardation effect in-

[a]Author to whom correspondence should be addressed; electronic mail: bonafos@cemes.fr
[b]On leave from Ioffe Physico-Technical Institute, St. Petersburg 194021, Russia.

 © 2006 American Institute of Physics

creases when the NC size decreases, leading to a self-limiting oxide growth. The model predictions show a good agreement with the experimental results.

II. EXPERIMENTAL DETAILS AND METHODS

Silicon dioxide layers of 7 nm in thickness were thermally grown by dry oxidation on 8-in., *p*-type, (100)-oriented Si wafers, and subsequently implanted with 1 keV ^{28}Si ions to a dose of 10^{16} Si^+ cm^{-2} using an AXCELIS GDS-ULTRA implanter. Then, the implanted samples were cleaned using a piranha solution, annealed for 30 min at 1050 °C under N_2 for the purpose of NC formation, and thermal oxidized under $N_2+1.5\%$ O_2 at 900 °C for different times (from 5 to 240 min). Cross-sectional and plan-view TEM specimens were prepared by the standard procedures of grinding, dimpling, and Ar^+-ion-beam thinning. Due to the small difference in atomic number and density between Si and SiO_2, the NCs show a weak amplitude and phase contrast by TEM. Size distribution can be measured on high-resolution electron microscopy (HREM) images or by using dark-field conditions, but as these images are orientation dependent, the direct measurement of the NC surface density is impossible. Therefore, the Si NCs were imaged on a plan-view specimen by performing parallel electron-energy-loss spectroscopy (PEELS) in a scanning transmission electron microscope, VG-HB 501 operating at 100 kV, using the spectrum-image technique (called PEELS-STEM in the following).[18] This microscope is equipped with a field-emission cathode and a parallel Gatan 666 EELS spectrometer. The EELS spectra were recorded over the first 50 eV on each image point of the specimen (typically 256×256). The EELS experiment is performed in the low-energy-loss domain. Plasmons, corresponding to plasma oscillations of valence electrons associated with each phase of the analyzed area, are the major signatures in this energy domain of the EELS spectra. Bulk silicon and silica plasmons are located at 17 and 23.5 eV, respectively. They are well separated and thus can be used to get the image associated with the corresponding phase. After acquisition of a spectrum at each point of the image, contributions from silicon plasmon and silica plasmon are isolated by reconstruction of the signal with reference spectra of Si and silica. Then a map can be displayed where the gray levels are defined by the weight of Si deduced from the reconstruction parameters. On such "chemical images," all the Si NCs are visible, amorphous, eith crystalline, and in the last case whatever their orientation is. A contrast enhancement method is applied to these images in order to perform quantitative measurements such as the NC mean size and aerial density and surface fraction and number of atoms stored within the NCs. In order to control the homogeneity of the NC distribution throughout the plan-view TEM samples, energy filtering transmission electron microscopy (EFTEM) experiments have also been performed for particular samples. By inserting an energy-selecting slit in the energy-dispersive plane of the filter at the Si plasmon energy, the population of Si NCs can also be visualized. A TEM-FEG microscope, Tecnai F20ST equipped with an energy filter, TRIDIEM from Gatan was used. The contrast in the EFTEM raw images is less than in the PEELS-STEM technique because there is a contribution of the silica plasmon signal at the plasmon energy of Si. However, after applying the contrast enhancement method, the two types of images became comparable.

Cross-sectional TEM (XTEM) studies were carried out using a CM30 Philips TEM equipped with a LaB_6 cathode operating at 300 kV and having a nominal resolution of 0.19 nm. These observations aim at measuring the depth position of the NC layer in the SiO_2 layer and, in particular, the location of the NCs in respect to the Si substrate and the surface. For this, we have developed a method for fast and accurate distance measurements using Fresnel contrast.[19] As mentioned earlier, the difference between the mean atomic numbers and the densities in Si and SiO_2 are small so the Si NCs show no amplitude contrast when buried in a SiO_2 layer. Nevertheless, the electrostatic potentials being slightly different in Si and SiO_2, some small phase shift exists between electron waves having propagated or not through the NC layer. This phase shift can be "imaged" by using strongly defocused bright-field conditions, provided the incident beam is highly coherent. Under such conditions, a pair of (black/white or white/black) Fresnel fringes appears exactly centered on each interface. Microdensitometric analysis of such images can be performed using an online charge-coupled device (CCD) camera and image processing facilities so that averaging of the gray levels along the direction perpendicular to the layers can be represented by a "line scan." Thus, on such experimental densitometric profiles, all the distances of interest can be precisely measured by locating the inflexion points of each pair of black and white fringes originating from the different interfaces. The uncertainty of these distance measurements is estimated to be ±0.5 nm. Finally, a poly-Si layer has been deposited after annealing on top of the samples in order to facilitate the distance measurement with respect to the surface.

III. EXPERIMENTAL RESULTS

As shown in Ref. 20 the NC characteristics strongly depend on the implanted dose. When implanting at 1 keV no NCs are detected for doses below 5×10^{15} cm^{-2}, while a high dense array of spherelike NCs is formed at a medium dose (10^{16} cm^{-2}) and a connected array of elongated NCs with a larger size and less density is formed at a highest dose (2×10^{16} cm^{-2}). In the last case, annealing under N_2+O_2 has been shown to be an efficient way for separating the connected NCs.[21] In this work, we have chosen to study the oxidation process of Si NCs embedded in SiO_2 in the case of the medium range fluence (10^{16} cm^{-2}) for which a high density of well-separated spherical NCs is observed after annealing at 1050 °C for 30 min under N_2 [see Fig. 1(a)]. After this high-temperature NC formation step, the NCs were oxidized at 900 °C for different durations (between 5 and 240 min). As reported above, the oxidation temperature being above the viscoelastic temperature [950 °C for thermal SiO_2 (Refs. 11 and 12)], a self-limiting oxidation process is expected.[22,23] As it appears in the PEELS-STEM images of Fig. 1 and on the graph shown in Fig. 2(a), the average size of the NCs

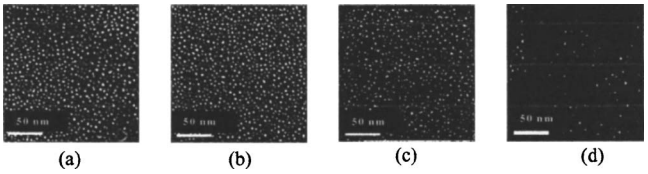

FIG. 1. Plan-view PEELS-STEM images of (a) reference sample (N_2); [(b)–(d)] oxidized samples after 5, 30, and 240 min, respectively. The contrast of the original images has been enhanced.

(square symbols) slowly decreases from 2.9±0.3 nm for the reference sample (N_2, 1050 °C, 30 min) to 1.8±0.2 nm for a sample annealed under N_2+O_2 during 240 min. Meanwhile, the NC density [see Fig. 2(b)] decreases by a factor of 10. Thus, the surface fraction (coverage) decreases from 12% after 5 min to 1% after 240 min of annealing [see Fig. 3(a)]. This corresponds to a decrease of the number of Si atoms by a surface unit contained within the NCs from 1.4×10^{15} to 10^{14} at. cm^2 [see Fig. 3(b)], indicating that the progressive oxidation of the nanoclusters takes place. As we can see in Figs. 2 and 3, this evolution takes place following two stages. During the first 60 min the size and NC density linearly decrease and then, for longer annealing times, the consumption of silicon slows down and stabilizes.

XTEM observations (see Fig. 4) have allowed the measurement of the different characteristic distances—SiO_2 thickness (e_{SiO_2}), injection distance (d_{inj}, SiO_2 thickness between the Si/SiO_2 interface and the NC layer), width of the NC layer (e_{ncs}), and gate distance (d_{gate}, SiO_2 thickness between the NC layer and the SiO_2 surface)—by using the method described in Ref. 19. The cross-sectional scheme in Fig. 5 shows the quantitative evolution of these distances (x axis) for different annealing durations (y axis). As we can see in Fig. 5, the width of the NC layer slightly decreases with an increase of the annealing time under N_2+O_2. For oxidation duration larger than 30 min, the contrast of the NC layer is very weak, due to the small density of particles, and the evaluation of the NC layer width is no more possible. On the other hand, the whole oxide thickness increases when increasing the oxidation duration (from 10.4±0.5 initially to 13.2±0.5 nm after 240 min). It is important to point out that this swelling concerns both the control and the injection oxide: the SiO_2/Si interface is therefore also oxidized in addition to the NCs.

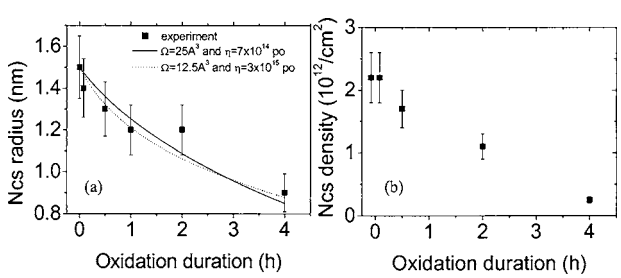

FIG. 2. Evolution of (a) the Si NC mean radius and (b) of the NC aerial density vs annealing time under N_2+O_2, as measured on the images in Fig. 1. In (a) the model predictions for $\Omega=25$ Å^3 and $\Omega=12.5$ Å^3 are plotted in the solid and dashed lines, respectively.

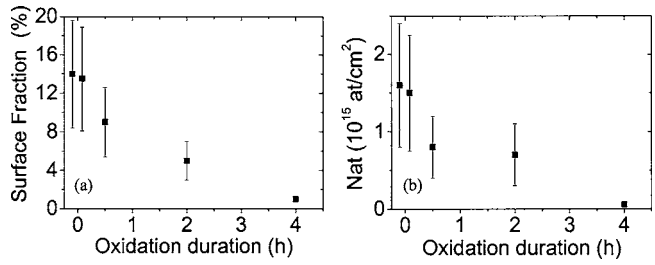

FIG. 3. Evolution of (a) the percentage of surface occupied by Si NCs (coverage) and (b) of the number of silicon atoms within the NCs vs the annealing time under N_2+O_2, deduced from the images in Fig. 1.

IV. MODELING OF THE SI NANOCRYSTAL OXIDATION

The most comprehensive characterization of the stress effects during oxidation of nonplanar Si structures was performed by Kao *et al.*[13,14] These authors have extended the one-dimensional stress-free model of Deal and Grove[17] to the oxidation of nonplanar silicon structures, i.e., to concave and convex cylindrical 2D structures. For this, they treated the oxide as an incompressible viscous fluid being driven by a velocity field at the silicon/oxide interface.

This assumption (SiO_2 is a viscous fluid) is, in fact, valid above the viscous flow point (950 °C), while at low temperatures (below 800 °C) SiO_2 behaves as an elastic solid.[11,12] Between these extremes, it presents more complex mechanical characteristics and for modeling stress effects during nonplanar oxidation, several authors have considered a viscoelastic behavior, which mixes both reversible elastic deformation and steady flow process.[24]

A further improvement of the modeling of stress effects in silicon oxidation led to the introduction of shear-stress-dependent viscosity.[24–26] This stress effect is, in fact, similar to a plastic phenomenon and gives a nonlinear behavior to the material. Indeed, it is known from the experiment that SiO_2 becomes more fluidic under a high stress state,[27] leading to a strong modification of its viscosity. The lowered viscosity at a high stress level results in a slower increase of the oxide stress when increasing the interfacial curvature than would otherwise occur. Plasticity has been incorporated in both viscoelastic and viscous formulations.[24–26,28] For 2D cylinders, it has been shown that linear viscous models usually overpredict the stress by two orders of magnitude at low temperature even if the viscoelastic solution approaches the plastic solution at high temperature.[28] In addition, still for 2D structures, the linear viscous flow models generate stress values larger, especially at low temperatures, than the threshold value for plastic deformation (for SiO_2 10^9 dyn/cm^2, i.e., 10^8 Pa).[28] At last, taking into account nonlinearity deformation has been proven to be crucial for the successful fitting of the experimental results for concave structures.[25,26]

In our experimental case (dry oxidation at 900 °C for

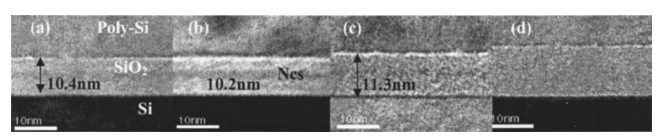

FIG. 4. XTEM images of (a) reference sample (N_2); [(b)–(d)] oxidized samples for 5, 30, and 240 min, respectively.

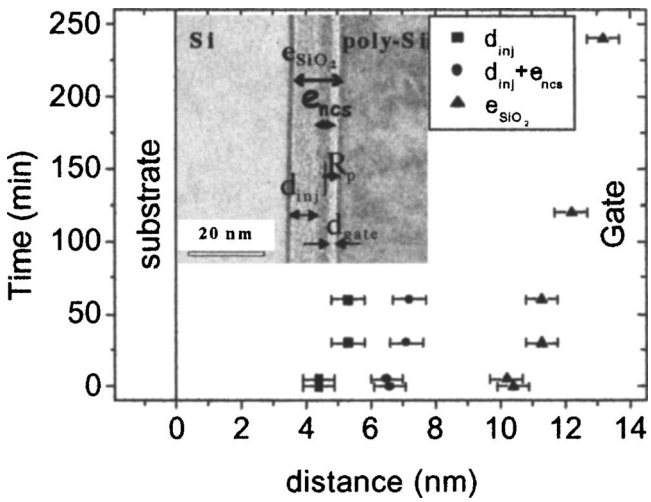

FIG. 5. Cross-sectional scheme depicting the evolution of the characteristic distances as a function of the oxidation duration, from 0 (reference sample) to 240 min at 900 °C (y axis). These distances were measured on the XTEM images of Fig. 4 and are plotted on the x axis. Up triangles: distance between the bottom edge of the NC layer and the Si substrate (injection distance). Down triangles: distance between the top edge of the NC layer and the Si substrate. Squares: distance between the polysilicon layer and the Si substrate (SiO_2 thickness). All the distances are measured with an accuracy of ±0.5 nm. In the inset, a XTEM image is shown where all these distances are defined.

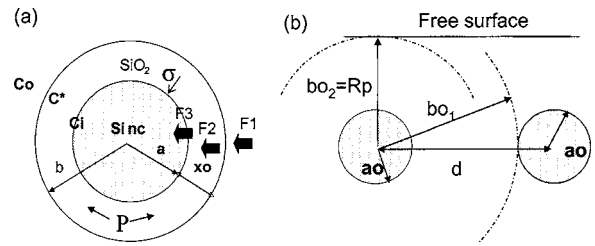

FIG. 6. Schematics of (a) a spherical Si NC surrounded by an oxide shell with normal compressive stress at the interface (σ) and tensile stress (hydrostatic pressure, P) within the oxide volume, which appear during the viscous flow of the growing oxide and (b) of two neighboring NCs surrounded by their oxide shell.

some hours) we have evaluated by a simple calculation the time for viscous flow to develop, that is, the time for the stress to reach the steady-state value.[29] This time is, by using a linear model and viscosity values measured by Fargeix and Ghibaudo,[30] of about 50 min, i.e., smaller than the whole oxidation duration (some hours). As a consequence, we have assumed in our model a deformation of SiO_2 by viscous flow. This assumption is in agreement with EerNisse's experimental measurements[11] of diagnostics viscous flow of dry and wet SiO_2 when annealing at 925 °C for oxidation times larger than 20 min. In addition, we have considered that the thermal budget (900 °C for some hours) was sufficiently high that we can neglect plastic deformation and assume linear deformation and a pressure-dependent viscosity, as described by Dane and Birch[31] and not a shear-modulus-dependent viscosity linked to plasticity effects.[24–26] In other words, we treated the oxide as an incompressible viscous fluid as Kao *et al.*[13,14] and Omachi *et al.*[16] also did. The obtained stress levels will be discussed in Sec. V and compared to the threshold stress value for plastic deformation.

The 2D model of Kao *et al.*,[13,14] which concerns the micrometric concave and convex cylindrical structures under wet oxidation, has been extended to the three-dimensional (3D) spherical conditions by Chen and applied to nanocrystalline Si quantum dots under dry oxidation.[15] To avoid a tedious fluid mechanics analysis of oxide stress, these authors have used an approximate scale analysis and assumed the influence of stress on the diffusion and solid solubility constant to be much less important than the influence on the chemical reaction rate. Omachi *et al.*[16] have included these effects in their model. Nevertheless, their model implies not less than five fitting parameters and a good agreement with the experiment is obtained for values of the zero-pressure viscosity of 10^{12} poises, i.e., three orders of magnitude less than measured at this temperature (850 °C) for dry oxidation.[30]

To model the oxidation process of our system, i.e., Si NCs embedded within a thin SiO_2 matrix, we have used the extension of the Deal and Grove model to 3D geometry of Omachi *et al.*,[16] implying both normal stress at the interface and hydrostatic pressure in the oxide volume. A particular attention has been paid in limiting the number of fitting parameters and in using realistic constants. This model predicts the evolution during annealing under oxidizing ambient of a NC with an initial size, the average radius of the NC population after the nucleation stage (reference sample).

Classically, the oxidation is divided into three processes which are associated with three fluxes [see Fig. 6(a)].[17] The first flux F_1 concerns the diffusion of oxidizing species (O_2) at the gas/oxide interface, the second flux F_2 is associated with the diffusion of the oxidizing species into the SiO_2, and the third flux F_3 represents the flux of oxidizing species at the Si/SiO_2 interface. These three fluxes can be expressed as

$$F_1 = h(C^* - C_0), \tag{1}$$

$$F_2 = -D\frac{dC}{dr}, \tag{2}$$

$$F_3 = k_s C_i, \tag{3}$$

where h is the surface mass transfer constant of oxidant, D is the diffusivity of oxidant in the SiO_2, k_s is the surface reaction rate constant at the SiO_2/Si interface, C^* is the oxidant solubility in SiO_2, C_i is the concentration of oxidant near the Si/SiO_2 interface, and C_0 is the concentration of the oxidant at the outer surface of the oxide.

In the Deal and Grove model, the three fluxes are set equal due to the steady-state condition. The steady-state diffusion equation inside the oxide is given by

$$\nabla^2 C = \frac{1}{r^2}\frac{\partial}{\partial r}\left(r^2\frac{\partial C}{\partial r}\right) = 0. \tag{4}$$

The solution of this Laplace equation in spherical coordinates is a hyperbole fragment, $C(r)=A+B/r$. Considering that the mass transport is conserved for any radius r and combining Eqs. (1)–(4) the oxidation rate for a spherical Si NC can be expressed as[15,16]

$$\frac{dx}{dt} = \frac{1}{N}\frac{C^*}{1/k_s + a^2/b^2h + a(b-a)/bD}. \quad (5)$$

Instead of

$$\frac{dx}{dt} = \frac{1}{N}\frac{C^*}{1/k_s + 1/h + (1/D_0)(b-a)}$$

for planar oxidation.[17] $x=b-a$ with a is the NC core radius and b is the radius of the NC core plus oxide shell [see Fig. 6(a)], both varying with time. N is the number of oxidant molecules incorporated into SiO_2 per unit volume of oxide grown. $N=2.2\times10^{22}$ molecules/cm^3 for dry oxidation by considering that one O_2 molecule is incorporated into each SiO_2 molecule. Because of volume conservation, the Si core radius, a, and the core + shell radius, b, are not independent variables.[15] We assume an incompressible fluidic oxide and the ratio of produced SiO_2 volume to the consumed Si volume 2.25(=45/20): 1. If the starting radius of Si core is a_0 and the starting radius of the core + shell sphere is b_0, the above assumption results in the following relation between a and b:[15]

$$b^3 + 1.25a^3 = b_0{}^3 + 1.25a_0{}^3 = B. \quad (6)$$

The evolution of the new NC radius $a(t)$ is thus given by

$$\frac{da}{dt} = -\frac{dx}{dt}\frac{1}{1+1.25a^2(B-1.25a^3)^{-2/3}}. \quad (7)$$

As shown by Kao *et al.*,[13,14] the oxidation of non-planar-structured Si must take into account the influence of stress at the Si/SiO_2 interface. Indeed, as the volume of grown oxide is larger than the initial volume of Si, the material should expand. As a result, the newly formed oxide pushes the old one which rearranges itself through viscous flow. The structure relaxes towards equilibrium according to the mechanical properties of the oxide which are characterized by fluid deformations. Following Kao *et al.*,[13,14] two types of stress are generated that retard the oxidation process. One is the normal compressive stress σ generated at the Si NC/SiO_2 interface and the other one is the tensile stress P (hydrostatic pressure) generated in the oxide shell [see Fig. 6(a)].

For 3D structures, the normal stress at the Si NC interface is given by[15,16]

$$\sigma = -4\eta\beta\left(\frac{1}{a^3} - \frac{1}{b^3}\right), \quad (8)$$

where η is the viscosity and β is the velocity constant, which is a function of the oxide velocity at the interface. Based on the work of Omachi *et al.*,[16] we take the following sign convention for stress: positive for tension and negative for compression. The effect of this normal stress is to reduce the surface reaction rate (k_s) by adding to activation energy the extra work which has to be carried out by the expanding oxide,[13–16]

$$k_s = k_{so}\exp\left(\frac{\sigma\Omega}{kT}\right), \quad (9)$$

with Ω the volume expansion and k_{so} the stress-free value of k_s.

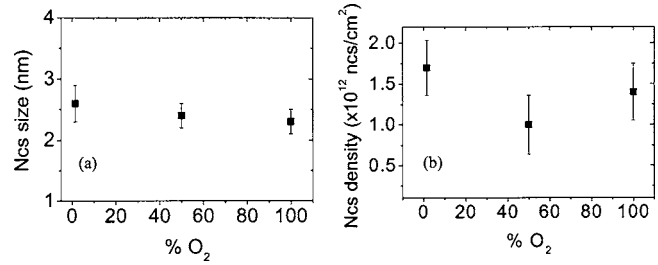

FIG. 7. Evolution of (a) the NC mean radius and (b) NC density vs the O_2 content, as measured on plan-view PEELS-STEM images. The samples have been implanted at 1 keV with a dose of 2×10^6 cm^{-2}, annealed under N_2 during 30 min at 1050 °C and under N_2-diluted O_2 with 1.5% O_2, 50% O_2, and 100% O_2 at 900 °C for 30 min.

For planar oxidation, k_{so} varies with the oxygen partial pressure.[17,32,33] Nevertheless, the NC population is found the same in the experimental error bars (in average size and aerial density) when oxidizing under 1.5% of O_2 and 100% O_2 (see Fig. 7). The oxidation of the particles is therefore independent of the O_2 content. As a consequence, k_{so} has been taken here independent of the oxygen partial pressure. The parameter Ω has the physical significance of the reaction jump volume in the Si to SiO_2 transition. The model states here that the oxidizing species need to have enough energy to move the newly formed oxide against the normal force field σ. The energy required in a unit reaction is the product of the reaction jump volume Ω and σ. Initially, Ω was taken equal to $\Omega_{SiO_2}-\Omega_{Si}=25$ Å^3,[13–16] while Sutardja *et al.*[25] and Sutardja and Oldman[26] argued that a unit reaction involves the breaking of one Si–Si bond and the attachment of a bridging oxygen atom between the two Si atoms. In this case, Ω must be close to 12.5 Å^3, the difference between the volume of Si–O and Si. In our model, these two cases have been considered. This normal stress makes the reaction at the silicon NC surface more difficult and affects the surface reaction rate which decreases as the normal stress compressively increases.

The hydrostatic pressure in the oxide volume (P) is given by[16]

$$P = 4\eta\beta\frac{1}{b^3}. \quad (10)$$

This stress is created in the bulk of the old oxide which is stretched and being pushed out and is tensile for convex surfaces. The diffusivity D and the solubility C^* of the oxidant are increased by tension while it is the opposite for the viscosity η,[13,14,16]

$$D = D_0\exp\left(\frac{PV_a}{kT}\right), \quad (11)$$

$$C^* = C_0{}^*\exp\left(\frac{PV_s}{kT}\right), \quad (12)$$

$$\eta = \eta_0\exp(-\alpha P), \quad (13)$$

where D_0, $C_0{}^*$, and η_0 are, respectively, the zero-pressure diffusivity, solubility, and viscosity. V_a and V_s are the activation volumes of diffusivity and solubility. α is an empirical

parameter. We assume here the pressure-dependent oxide viscosity model proposed by Kao *et al.*[13,14] As the tensile stress increases the O_2 diffusivity and solubility increase while the viscosity decreases. Then, the oxidant transport and the viscous flow are enhanced comparing to zero-pressure conditions. The two stresses σ and P are functions of viscosity which has a strong temperature dependence. Therefore, the normal and hydrostatic stresses are both higher at low temperatures for which the viscosity is much larger and it is more difficult for the oxide to flow. By taking into account these stress effects, the oxidation rate can be written as

$$\frac{dx}{dt} = \frac{C_1 \exp(\sigma\Omega/kT)}{1 + \exp(\sigma\Omega/kT)\{(a^2/b^2)C_2 + [a(b-a)/b]C_3\}}, \quad (14)$$

with

$$C_1 = C_{10} \exp\left(\frac{PV_s}{kT}\right) \quad \text{and } C_{10} = \frac{C_0^* k_{so}}{N} = \left(\frac{B}{A}\right)_{\mathrm{DG}}, \quad (15)$$

$$C_2 = C_{20} = \frac{k_{so}}{h}, \quad (16)$$

$$C_3 = \frac{C_{30}}{\exp(PV_a/kT)} \quad \text{and } C_{30} = \frac{k_{so}}{D_0} = 2\left(\frac{B}{A}\right)_{\mathrm{DG}} \Big/ B_{\mathrm{DG}}. \quad (17)$$

C_{10} and C_{30} are deduced from the linear and parabolic constants $(B/A)_{\mathrm{DG}}$ and B_{DG} of the 1D Deal and Grove (DG) oxidation model[17] and depend only on the temperature and Si orientation. We considered here for the dots a (111) orientation even if they are, in fact, randomly oriented. Indeed, for this orientation the oxidation velocity ranges in between the velocity for (110) orientation, which is the fastest and the one for (100) orientation, which is the slowest. C_{20} is more problematic to evaluate as depending on h, the gas-phase mass transfer coefficient, which is a function of the furnace configuration. Nevertheless, in our calculation, the term depending on C_2 is always negligible, when considering classical values for h, taken from the literature.[15,17]

The time evolution of the oxidation rate is solved by means of a Runge-Kutta method. The initial values of a and b are taken from the experiment: $a_0 = 1.5$ nm is the NC mean radius for the reference (nonoxidized) sample, as measured on the images in Fig. 1. Our system differs from those previously studied in the literature because the NCs are embedded within SiO_2 and not deposited on top of it. Indeed, in our case a shell of SiO_2 surrounds the NCs before the beginning of the oxidation process and this shell is larger than the NC radius itself. This oxide shell is anisotropic in dimension as the average distance between the NCs (lateral distance, d) can be different from the distance of the precipitates to the free surface (perpendicular distance, R_p), see Fig. 6(b). The average distance (d) between the precipitates can be calculated from the NC density and ranges between 4 and 6 nm following the model considered (hexagonal-type compact stacking or a classical cubic one). This leads to an oxide shell $b_{0_1} = d - a_0$ ranging from 3 to 5.5 nm [see Fig. 6(b)]. On the other hand the distance of the NCs to the surface (perpendicular distance) can be measured on XTEM images and is $b_{0_2} = R_p = 4.5 \pm 0.5$ nm. This value ranges in between the two values found for b_0 when considering lateral distances. Therefore the anisotropy of the system is not very important (1.5 ± 0.5 nm). Finally, the impact of the initial value of the oxide shell (b_0) on the simulation has been tested and we have seen that a decrease of b_0 leads to an increase of the viscosity (and inversely) to fit the experimental evolution. Anyway, these viscosity values always range in the expected ones at this temperature.[30] We have taken in our model $x_0 = b_0 - a_0$ on the order of the control gate oxide thickness at $t=0$, and therefore $b_0 = 4.5$ nm (perpendicular distance), as measured in the XTEM images in Fig. 4.

Omachi *et al.*[16] used the activation volumes of solubility and diffusivity, V_s and V_a, respectively, as fitting parameters. For wet oxidation, Kao *et al.*[13,14] have shown that V_s must be of the same order of magnitude as the molecular volume of H_2O. In this direction, we have considered V_s of the order of magnitude of the molecular volume of O_2, i.e., 20 Å^3,[34] for dry oxidation. Concerning V_a, a large range of values can be found in the literature, from 75 to 600 Å^3.[16,24,25] These values are deduced by experimental data fitting. By using V_a in the 75–600 A^3 range, our simulation results indicate that this parameter has no significant impact on the oxidation rate. As a consequence, the zero-pressure viscosity, η_0, and the pressure coefficient for viscosity, α, are the only fitting parameters needed in our model for describing the thermal oxidation of NCs.

Also, by considering these input values, we obtain $\exp(\sigma\Omega/kT)\{(a^2/b^2)C_2 + [a(b-a)/b]C_3\} \ll 1$, i.e., $1/k_s \gg a^2/b^2h + a(b-a)/bD$. In other words, the oxidation process does not depend on the diffusion coefficient and is only a function of k_s, the surface reaction rate. The oxidation is therefore reaction limited, as it is the case in planar oxidation for thin oxides.[17]

Under this condition, the expression of the oxidation rate can be simplified to

$$\frac{dx}{dt} = C_{10} \exp\left(\frac{PV_s}{kT}\right) \exp\left(\frac{\sigma\Omega}{kT}\right). \quad (18)$$

V. COMPARISON OF THEORY AND EXPERIMENTS

Concerning the evolution of the NC mean radius during oxidation, as mentioned in Sec. III, we observe that the size of the NCs decreases and saturates when increasing the oxidation time. This evidences that the oxidation rate slows down as the silicon nanocluster radius becomes smaller, i.e., that we have a self-limited oxidation process. In the case of $\Omega = 25$ Å^3, we obtain a good agreement between our model and the experimental data [see Fig. 2(a) in solid line] for a viscosity of $\eta_0 = 7 \times 10^{14}$ poises and for $\alpha = 1.5 \times 10^{-8}$ Pa^{-1}, i.e., of the order of magnitude of the one proposed in Refs. 13 and 16. When taking $\Omega = 12.5$ Å^3, the model fits with the experimental results for a value of viscosity of 3×10^{15} poises [see Fig. 2(a) in dashed line]. These values of viscosity are very close to the one found by Fargeix and Ghibaudo (1.5×10^{15} poises) for dry oxides.[30] While the value taken for α has no strong impact on calculation, this is not the case for

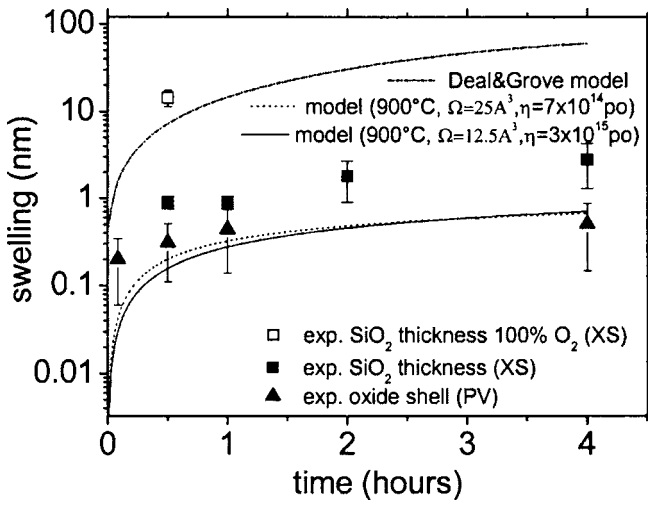

FIG. 8. Experimental evolution vs annealing time of the swelling with respect to the nonoxidized sample of the whole SiO_2 layer measured in XTEM (plain squares for 1.5% O_2 and empty squares for 100% O_2) and of the thickness increase of the SiO_2 shell generated by the Si NC oxidation, as deduced from plan-view measurements (up triangles). In the dot-dashed line is plotted the model predictions for planar oxidation (1D Deal and Grove model) and in the solid and dashed lines our model results for 3D oxidation (for, respectively, $\Omega=25$ Å^3 and $\Omega=12.5$ Å^3).

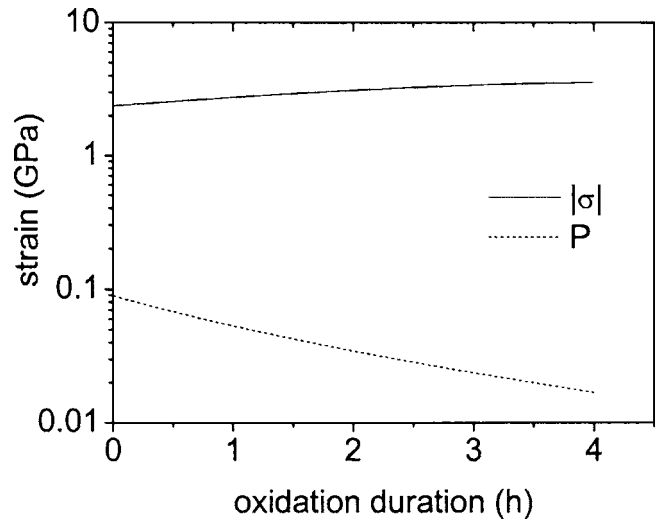

FIG. 9. Evolution of compressive stress σ (in absolute value) and tensile stress P vs the annealing time for $\Omega=25$ Å^3.

the zero-pressure viscosity (η_0) at low temperatures; the smaller is the viscosity, the faster is the oxidation. As a consequence, the only parameter that affects oxidation is η_0. The agreement between our experimental data and simulation for realistic values of the viscosity renders our model credible.

The oxide shell dimension $(b-a)$ can be deduced from the experiment by subtracting the average volume of the NCs before and after each step of oxidation, calculated from the experimental mean radius and taking into account the corresponding volume expansion. The evolution of this shell dimension is plotted in Fig. 8 with triangle symbols. We observe a good agreement between the shell values predicted by our model (Fig. 8, solid and dashed lines following the value of Ω) and the experimental values. As already emphasized in Refs. 16, 22, 23, and 35, the oxidation of 3D NCs is slower than the one predicted by the classical Deal and Grove model for a planar interface, as plotted in the dot-dashed line in Fig. 8.[17] This theoretical evolution even underestimates the oxidation rate which is enhanced for thin oxides (below 25 nm).[36] We can also notice that, for oxidation times larger than 5 min the expansion of the whole SiO_2 layer (square symbols in Fig. 8), deduced from Fig. 5, is much larger than these shell values (triangle symbols in Fig. 8). This discrepancy is due to the SiO_2/Si interface oxidation already mentioned in Sec. III. Anyway, this interface oxidation is several times smaller than the one predicted by the planar oxidation Deal and Grove model (dot-dashed line).[17] This can be explained by the percentage of O_2 which is 1.5% instead of 100%. Indeed, if there is no effect of the O_2 pressure on the NC reaction rate because the oxidation process is mainly limited by the stress effects, this is not the case for the oxidation rate of the SiO_2/Si substrate interface. By comparison, the oxide swelling for the sample annealed with 100% O_2 at 900 °C for 30 min (open square in Fig. 8) is 10 ± 0.5 nm larger than the one for the 1.5% O_2 at this thermal budget. This expansion is even larger than the one expected by the Deal and Grove theory, as predicted by Massoud *et al.*[36]

In Fig. 9, we have plotted the compressive normal stress σ at the interface of the NCs (in absolute value) and the tensile stress in the oxide bulk (hydrostatic pressure) P in the bulk oxide predicted by the model during oxidation. When increasing the oxidation duration, σ increases in absolute value, leading to a decrease of the reaction rate k_s and therefore a retardation of the oxidation process. On the other hand, the tensile stress in the volume, P, decreases during oxidation, leading to a decrease of the O_2 diffusivity and solubility, even if both of them remain larger than the values at zero pressure. In particular, the decrease of the solubility during oxidation contributes to the retardation of the oxidation process. The decrease of the hydrostatic pressure during oxidation also leads to an increase of the viscosity that increases the normal strain at the interface (in absolute value) and therefore contributes also to the retardation of the oxidation process.

A good agreement between our model and the experimental evolution is obtained by considering both the effect of the normal stress at the interface (σ) and the stress in the volume (P). When considering only one of these two stresses the model fails in describing the experimental evolution. When taking into account P only while the oxidation rate is several times faster than when taking into account both P and σ. For σ only, a quasilinear evolution of the NC radius is found and fails in fitting the experimental evolution, whatever the considered viscosity and volume expansion (Ω).

For the considered viscosity, the values of the compressive stress at the interface and the tensile stress in the oxide volume are of the order of some 10^9 and 10^8 Pa, respectively, and this, for the two values considered for Ω. These stress values are of the order of magnitude of the ones obtained by Dalla Torre *et al.* by using Monte Carlo calculation of the oxidation of very small Si NCs.[34]

We carried out all the calculations in this model assuming Newtonian flow of the oxide but, as mentioned in Sec.

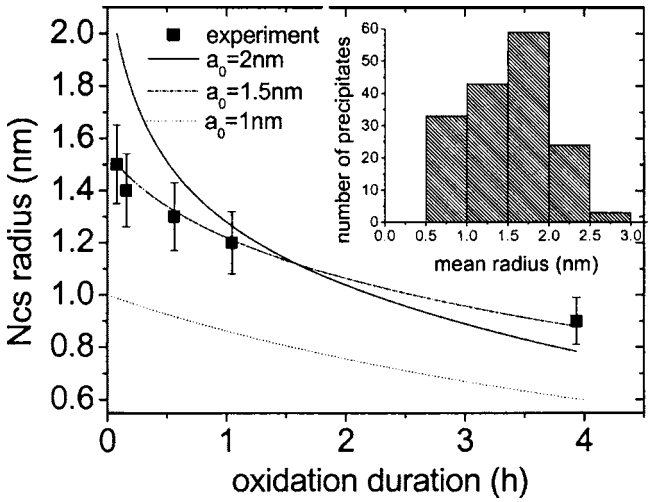

FIG. 10. Simulation of the evolution of the NC mean radius during oxidation for the different classes of size (a_0=1 nm, a_0=1.5 nm, and a_0=2 nm) encountered in the initial size histogram, shown in the inset, of the reference sample (nonoxidized). The simulations have been carried out with $\Omega = 12.5$ Å^3 and $\eta_0 = 1.5 \times 10^{15}$ poises.

IV, it was observed that at high temperature the flow of glasses is nonlinear at high stresses.[24–26,28] The stress level is here larger than that critical stress for nonlinear behaviors ($\sigma_c = 10^8$ Pa), suggesting that our model is limited and that the plastic flow should be considered. Nevertheless, this critical stress value, used in the actual plastic models, is measured for silica glass for which the viscosity and the glass transition temperature are different from dry thermal SiO_2.[37] It is therefore difficult to take this value as an absolute threshold. In addition, the stress values that we obtained are in good agreement with those measured by Raman for NC ion beam synthesized in SiO_2 ($\sim$1 GPa),[38] and this stress level is still lower than the threshold value for the fracture of a Si wafer (10–25 GPa).[39]

A last point to clarify lies in the important decrease of the NC aerial density, which falls down from 2.2 ($\pm$0.4) $\times 10^{12}$ to 2.5 ($\pm$0.5) $\times 10^{11}$ cm^{-2}, as experimentally observed on Fig. 2(b). Even if the average diameter of the NCs decreases down to 2 ± 0.2 nm, this value is still larger than the visibility threshold in the PEELS-STEM images, which lies around 1 nm. Nevertheless, the NCs are size distributed (see inset of Fig. 10 for the nonoxidized sample) and the simulation of Fig. 2(a) (or reported in the dot-dashed line in Fig. 10) concerns only the NCs having the average size of the population (1.5 nm). The NCs initially larger than the average size, for instance, those having a radius of 2 nm, are shrinking faster as their initial oxidation velocity is higher (see Fig. 10 in solid line). For this reason, after 100 min of annealing, their size is smaller than the one reached by the NCs starting with a radius of 1.5 nm.

Anyway, even if shrinking faster, they are still larger than the visibility limit at the end of the oxidation. On the other hand, around 50% of the NCs for the nonoxidized sample are smaller than the average size (see inset of Fig. 10). The simulation of the oxidation of precipitates having 1 nm in diameter is also shown in Fig. 10 (dashed line). After 240 min of annealing, this class of NCs has an average diameter of around 1.2 nm, i.e., close to the visibility limit. We can consider therefore that 50% of the NCs have disappeared during the oxidation annealing. This dissolution does not explain the decrease of 90% in density observed in Fig. 2(b) but one has to take into account that during annealing the NCs naturally encompass a competitive growth called Ostwald ripening[40] where the NC density naturally decreases. A study of the evolution of the NC population, when annealing in this range of temperature under N_2 only, shows a natural decrease of the NC density of 40% while the mean radius only slightly increases, due to a nonconservative ripening process. The important decrease of the density as observed in Fig. 2(a) can be therefore attributed to the cumulative effect of these two processes.

VI. CONCLUSION

In conclusion, thermal treatments in N_2-diluted O_2 at a temperature below the viscoelastic temperature of SiO_2 (950 °C) appear to be a powerful way for manipulating the size distribution and surface density of 2D arrays of NCs embedded in thin SiO_2 films. Our experiments performed at 900 °C in 1.5% O_2 reveal that the NC mean size, density, and surface fraction significantly decrease with annealing duration, while the oxidation rate of the NCs slows down with time and stabilizes after 1 h annealing, thus indicating a self-limiting oxidation process. The Si substrate/SiO_2 interface is also oxidized but at a rate slower than the one predicted for planar oxidation. This discrepancy is due to the limited O_2 content used in our experiments. The effect of thermal oxidation on the Si NC size can be predicted by means of an extended spherical Deal-Grove model taking into account a stress-induced retardation process. The oxidation process is reaction limited and both (a) normal stress at the Si NC interface that retards the reaction rate constant k_s and (b) tensile stress in the bulk oxide that modifies the oxide viscosity and oxygen solubility in the oxide must be considered. The reaction rate being strongly limited by these stress effects, the O_2 percentage has no effect on the NC oxidation itself. The stress values required in our 3D model are smaller than the threshold for Si wafer fracture, but high enough for suggesting that possible effects of plasticity occur during SiO_2 deformation. This last phenomenon is under investigation and will be discussed in detail later together with the thermal oxidation of NCs at temperatures above the viscoelastic point. Finally, the electrical properties of the NC gate stacks herein reported have been studied and will be published in the close future.

ACKNOWLEDGMENTS

The authors would like to thank V. Soncini from ST Microelectronics Agrate for the oxidized wafers, A. Agarwal from Axcelis Technologies Inc. for the implantations, and M. Tencé and C. Colliex from LPS Orsay for PEELS-STEM images. The authors also gratefully acknowledge C. Krzeminski from IEMN Lille for fruitful discussions on the kinetics of oxidation.

[1]S. Tiwari, F. Rana, H. I. Hanafi, A. Hartstein, E. F. Crabbé, and K. Chan, Appl. Phys. Lett. **68**, 1377 (1996).
[2]G. Ammendola *et al.*, J. Vac. Sci. Technol. B **20**, 2075 (2002).
[3]Y. C. King, T. J. King, and C. Hu, IEEE Trans. Electron Devices **ED-48**, 696 (2001).
[4]H. I. Hanafi, S. Tiwari, and I. Khan, IEEE Trans. Electron Devices **43**, 1553 (1996).
[5]P. Normand, D. Tsoukalas, E. Kapetanakis, J. van den Berg, D. G. Armour, J. Stoemenos, and C. Vieu, Electrochem. Solid-State Lett. **1**, 88 (1998).
[6]P. Normand *et al.*, Nucl. Instrum. Methods Phys. Res. B **178**, 74 (2001).
[7]C. Bonafos, M. Carrada, N. Cherkashin, H. Coffin, D. Chassaing, G. Ben Assayag, and A. Claverie, J. Appl. Phys. **95**, 5696 (2004).
[8]P. Normand *et al.*, Appl. Phys. Lett. **83**, 168 (2003).
[9]P. Dimitrakis *et al.*, Solid-State Electron. **48**, 1511 (2004).
[10]H. Coffin *et al.*, Mater. Res. Soc. Symp. Proc. **830**, D6.6 (2005).
[11]E. P. EerNisse, Appl. Phys. Lett. **30**, 290 (1977).
[12]E. P. EerNisse, Appl. Phys. Lett. **35**, 8 (1979).
[13]D. B. Kao, J. P. McVittie, W. D. Nix, and K. C. Saraswat, IEEE Trans. Electron Devices **ED-35**, 25 (1988).
[14]D. B. Kao, J. P. McVittie, W. D. Nix, and K. C. Saraswat, Tech. Dig. - Int. Electron Devices Meet. **1985**, 388.
[15]Y. Chen, Microelectron. Eng. **57–58**, 897 (2001).
[16]J. Omachi, R. Nakamura, K. Nishiguchi, and S. Oda, Mater. Res. Soc. Symp. Proc. **638**, F531 (2001).
[17]B. E. Deal and A. S. Grove, J. Appl. Phys. **36**, 3770 (1965).
[18]C. Jeanguillaume and C. Colliex, Ultramicroscopy **28**, 252 (1989).
[19]G. B. Assayag, C. Bonafos, M. Carrada, A. Claverie, P. Normand, and D. Tsoukalas, Appl. Phys. Lett. **82**, 200 (2003).
[20]T. Müller *et al.*, Appl. Phys. Lett. **85**, 2373 (2004).
[21]C. Bonafos *et al.*, Mater. Res. Soc. Symp. Proc. **830**, D5.2 (2005).
[22]H. I. Liu, D. K. Biegelsen, N. M. Johnson, F. A. Ponce, and R. F. W. Pease, J. Vac. Sci. Technol. B **11**, 2532 (1993).
[23]K. C. Scheer *et al.*, J. Appl. Phys. **93**, 5637 (2003).
[24]V. Senez, D. Collard, B. Baccus, M. Brault, and J. Lebailly, J. Appl. Phys. **76**, 3285 (1994).
[25]P. Sutardja, W. Oldman, and D.-B. Kao, Tech. Dig. - Int. Electron Devices Meet. **1987**, 264.
[26]P. Sutardja and W. Oldman, IEEE Trans. Electron Devices **ED-36**, 2415 (1989).
[27]G. Hetherington, K. H. Jack, and J. C. Kennedy, Phys. Chem. Glasses **5**, 130 (1964).
[28]C. S. Rafferty and R. W. Dutton, Appl. Phys. Lett. **54**, 1815 (1989).
[29]C. S. Rafferty, L. M. Landsberger, R. W. Dutton, and W. A. Tiller, Appl. Phys. Lett. **54**, 151 (1989).
[30]A. Fargeix and G. Ghibaudo, J. Appl. Phys. **54**, 7153 (1983).
[31]E. B. Dane and F. Birch, J. Appl. Phys. **9**, 669 (1938).
[32]N. Lie, R. Razouk, and B. E. Deal, J. Electrochem. Soc. **129**, 2828 (1982).
[33]A. Reisman, E. H. Nicollian, C. K. Williams, and C. J. Merz, J. Electron. Mater. **16**, 45 (1987).
[34]J. Dalla Torre, *et al.* J. Appl. Phys. **92**, 1084 (2002).
[35]R. Okada and S. Lijima, Appl. Phys. Lett. **58**, 1662 (1991).
[36]H. Z. Massoud, J. D. Plummer, and E. A. Irene, J. Electrochem. Soc. **132**, 2685 (1985).
[37]P. P. Donnadieu, O. Jaoul, and M. Kleman, Philos. Mag. A **52**, 5 (1985).
[38]A. Wellner, V. Paillard, N. Cherkashin, C. Bonafos, H. Coffin, B. Schmidt, K. H. Heinig, and A. Claverie, J. Appl. Phys. **94**, 5639 (2003).
[39]J. Grisolia, G. B. Assayag, B. de Mauduit, A. Claverie, R. E. Kroon, and J. H. Neethling, Mater. Res. Soc. Symp. Proc. **681**, I3.2.1 (2001).
[40]C. Bonafos *et al.*, Nucl. Instrum. Methods Phys. Res. B **178**, 17 (2001).